Balancing ion transport and high-voltage stability in solvent-free UV-crosslinked PEO/PEC solid polymer electrolytes with succinonitrile

Journal of Power Sources 690 (2026) 240803

Contents lists available at ScienceDirect

Journal of Power Sources

journal homepage: www.elsevier.com/locate/jpowsour

Balancing ion transport and high-voltage stability in solvent-free UV-crosslinked PEO/PEC solid polymer electrolytes with succinonitrile

Francesco Gambino [a,b,*], Hamideh Darjazi [a,b], Giuseppe Antonio Elia [a,b], Claudio Gerbaldi [a,b,**]

[a] GAME Lab, Department of Applied Science and Technology (DISAT), Politecnico di Torino, Corso Duca degli Abruzzi 24, Torino, 10129, Italy
[b] National Reference Center for Electrochemical Energy Storage (GISEL) - INSTM, Via G. Giusti 9, Firenze, 50121, Italy

HIGHLIGHTS

- A solvent-free melt extrusion and UV curing strategy is introduced.
- SPEs are tuned via PEO/PEC ratio and SN incorporation.
- PEO/PEC (7:3) shows high ionic conductivity at 40 °C, ~4.8 V stability.
- Li||Li cells exceed 1400 h cycling, showing stable interfaces.
- Solid-state cells (LFP, NMC622) show high capacity and stability.

GRAPHICAL ABSTRACT

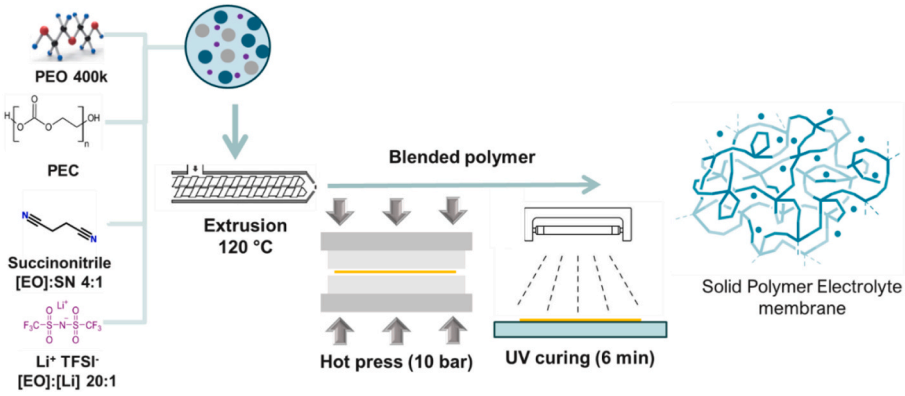

ARTICLE INFO

Keywords:
Solid polymer electrolyte
Succinonitrile
Crosslinking
Solvent-free extrusion
Lithium battery

ABSTRACT

Lithium metal batteries coupled with high-voltage cathodes offer outstanding energy density, but the development of solid polymer electrolytes (SPEs) simultaneously stable against lithium metal and oxidative cathodes remains a major challenge. Herein, a fully solvent-free route combining melt extrusion and UV curing is proposed to fabricate poly(ethylene oxide)-poly(ethylene carbonate) (PEO-PEC) SPEs plasticized with succinonitrile (SN). By tuning the PEO/PEC ratio and introducing SN, the electrolyte properties are optimized through the combined control of crystallinity, segmental mobility, and interfacial stability. Among the investigated formulations, the PEO/PEC 7:3 SPE encompassing SN exhibits the best overall performance, delivering practical ionic conductivity at 40 °C and anodic stability up to ca. 4.8 V vs. Li^+/Li. In symmetric Li||Li cells, the SPE enables continuous reversible lithium plating/stripping for more than 1400 h, maintaining moderate and stabilized polarization, and highlighting its enhanced compatibility with lithium metal. Its practical applicability is further demonstrated in

This article is part of a special issue entitled: MDB 2025 : Progresses and Challenges published in Journal of Power Sources.

* Corresponding author. GAME Lab, Department of Applied Science and Technology (DISAT), Politecnico di Torino, Corso Duca degli Abruzzi 24, 10129, Torino, Italy.
** Corresponding author. GAME Lab, Department of Applied Science and Technology (DISAT), Politecnico di Torino, Corso Duca degli Abruzzi 24, 10129, Torino, Italy.
E-mail addresses: francesco_gambino@polito.it (F. Gambino), claudio.gerbaldi@polito.it (C. Gerbaldi).

https://doi.org/10.1016/j.jpowsour.2026.240803
Received 17 April 2026; Received in revised form 17 June 2026; Accepted 22 June 2026
Available online 27 June 2026

truly all-solid-state Li-metal cells using both $LiFePO_4$ and NMC622 cathodes, which deliver full practical specific capacities and stable cycling at 40 °C. Overall, this work demonstrates that solvent-free reactive processing of SN-plasticized PEO-PEC SPEs is an effective strategy to mitigate the limitations of conventional polymer electrolytes and to enable high-energy density solid-state Li-metal batteries.

1. Introduction

Solid-state electrolytes (SSEs) are emerging as key components for lithium metal batteries (LMBs), which are considered among the most promising candidates for next-generation energy storage in electric vehicles, portable electronics, and grid-scale applications [1–3]. Interest arises not only from the possibility of coupling with lithium metal anodes to achieve higher energy density than conventional Li-ion batteries (LIBs), but also from the opportunity to improve battery safety. In contrast to LIBs based on flammable liquid organic electrolytes and porous separators, all-solid-state systems employ a solid electrolyte that can provide enhanced thermal stability, nonflammability, and non-volatility. These features are expected to mitigate electrolyte leakage and reduce the risk of thermal runaway, thereby improving the overall safety of the device [4–6].

SSEs can be classified into inorganic, polymer, and composite electrolytes. Ceramic electrolytes show high ionic conductivity, but are expensive and challenging to produce at scale [7]. Their brittle and rigid nature also makes conventional processing techniques, such as cutting or polishing, difficult, limiting practical application [8]. In contrast, solid polymer electrolytes (SPEs) are highly flexible, allowing adaptation to diverse battery geometries. In lithium metal polymer batteries, a lithium salt is homogeneously mixed with a suitable polymer, typically poly(ethylene oxide) (PEO) [9–11]. SPEs offer several compelling advantages for mobile device manufacturers, including high energy density, flexible design options, and improved safety compared to standard liquid electrolyte LIBs, owing to the absence or drastically reduced use of flammable organic solvents [12].

However, PEO-based SPEs exhibit relatively low lithium-ion conductivity at temperatures below their melting point (~60 °C), which significantly limits their practical application in all-solid-state batteries. In addition, oxidative degradation typically occurs above ~3.9 V vs. Li^+/Li, restricting their compatibility to lower-voltage cathodes such as $LiFePO_4$ [13]. To address these limitations, several strategies have been explored in the design of PEO-based SPE: i) introduction of plasticizers to increase the amorphous fraction and promote polymer segmental mobility; ii) incorporation of inorganic fillers to enhance chemical stability and provide additional ion-conduction pathways; iii) suppression of crystallinity through polymer blending or copolymerization.

To date, various plasticizers have been investigated to improve the ionic conductivity of PEO-based electrolytes. Conventional carbonate solvents such as EC, DMC, and PC are often introduced into SPEs to enhance ionic transport [14–16]. However, their inherent flammability raises serious safety concerns, as electrolyte combustion can initiate thermal runaway and its propagation within battery cells [17]. Ionic liquids (ILs) have also been considered as non-volatile alternatives to carbonate solvents. Nevertheless, certain ILs may exhibit toxicity depending on their cation-anion combinations, and their cost remains dependent on synthesis routes and large-scale production feasibility [18].

The incorporation of high-boiling, noncombustible organic plasticizers or ILs can substantially increase the amorphous fraction of PEO-based electrolytes, thereby facilitating faster Li^+ transport [19]. Among these, succinonitrile (SN) has emerged as a particularly effective solid-state plasticizer. SN possesses a plastic-crystalline structure that enables rapid Li^+ hopping conduction while maintaining structural stability [20,21]. Its strong dipolar –C ≡ N groups and dynamic lattice effectively suppress PEO crystallization and promote lithium salt dissociation, resulting in enhanced ionic conductivity within the polymer matrix [22,23]. Moreover, SN exhibits a wide electrochemical stability window exceeding 5 V vs. Li^+/Li, making it inherently compatible with high-voltage cathodes, such as NMC and LNMO [24,25]. These combined attributes position SN as an ideal additive to overcome the intrinsic conductivity and oxidative stability limitations of conventional PEO-based SPEs, while preserving the safety advantages of solid-state systems. Indeed, Xu et al. demonstrated that a high content of SN uniformly dispersed in SPEs can establish fast Li^+ migration pathways, as the molecular size of SN (~0.5 nm) closely matches the chain length of the EO units in PEO [26]. However, excessive SN loading (>10 wt%) has been shown to severely compromise the mechanical properties of the polymer matrix [27]. These findings highlight a critical trade-off: while plasticizers such as SN can markedly enhance ionic conductivity, they may simultaneously undermine structural integrity. To address this challenge, cross-linking strategies have been employed to construct a three-dimensional polymer framework that reinforces the matrix and preserves mechanical strength without sacrificing ionic transport [28,29].

Polymer blending, on the other hand, represents an effective strategy to simultaneously enhance structural integrity and electrochemical performance in SPEs. Aliphatic polycarbonates are attractive SPE matrices because their amorphous nature and carbonate moieties resemble conventional carbonate solvents, enabling high Li^+ transference numbers, broad electrochemical stability and good compatibility with Li metal. They can be used alone or blended with PEO, although their relatively high T_g generally penalizes ionic conductivity, especially at low salt content. In our previous work, PEO-poly(ethylene carbonate) (PEC) SPEs have been developed using a solvent-free extrusion process followed by UV-induced crosslinking (UV-curing, UV photopolymerization), demonstrating the feasibility of scalable solvent-free processing [30].

Building upon previous studies, here we introduce SN as a plastic-crystalline plasticizer into a UV-cured PEO-PEC matrix prepared through a fully solvent-free route. The combined incorporation of SN, optimization of the PEO-PEC composition, and formation of a cross-linked polymer network are designed to achieve high ionic mobility/transport at moderate temperatures while ensuring long-term interfacial stability against lithium metal. This design strategy aims to: (i) suppress polymer crystallinity and lower the glass transition temperature (T_g), thereby facilitating Li^+ transport at reduced temperatures; and (ii) expand the electrochemical stability window to enable compatibility with high-energy 4V-class cathodes. The resulting SPEs were systematically investigated using thermal analysis and vibrational spectroscopy to elucidate structural evolution, phase behavior, and intermolecular interactions within the polymer matrix. The controlled incorporation of SN significantly enhances ionic transport, electrochemical stability, and electrode–electrolyte interfacial compatibility, thereby improving electrolyte performance at 40 °C. The practical applicability of the developed system was further demonstrated through galvanostatic charge–discharge cycling of laboratory-scale LMBs even with high-energy-density 4V-class layered oxide cathodes, highlighting its potential for advanced SSLMBs.

2. Experimental

2.1. Materials

Poly(ethylene oxide) – PEO ($M_w = 4 \times 10^5$ g mol^{-1}, CAS 25322-68-3) was obtained from Merck. Poly(ethylene carbonate) – PEC

(M_w = 2.43 × 10^5 g mol^{-1}, CAS 25608-11-1) and poly((trifluoromethane)sulfonimide lithium methacrylate) – PMLiTFSI (M_n > 250 kDa, CAS 1818373-10-2) were received from Specific Polymers (France). Lithium bis(trifluoromethylsulfonyl)imide (LiTFSI, battery grade, CAS 90076-65-6), succinonitrile (SN, CAS 110-61-2), and 4-4′-difluorobenzophenone (99%, CAS 345-92-6), which is used as a photoinitiator, were provided by Merck. All polymers were dried for 3 days under vacuum at 60 °C; LiTFSI was dried under vacuum for one day at room temperature, two days at 70 °C, and finally 2 h at 110 °C. All drying procedures were carried out using a B-585 oven (Buchi Glass Drying Oven, Switzerland). Anhydrous N-methyl-2-pyrrolidone (NMP, CAS No. 872-50-4) was acquired from Merck and used as received. Conductive carbon black (C65, Imerys) and poly(vinylidene fluoride) (PVdF, Solef 6020, Solvay) were used without further purification. Lithium iron phosphate ($LiFePO_4$, LFP) cathode powder was provided by BASF. Lithium nickel manganese cobalt oxide (NMC622) cathode powder was provided by MSE Supplies.

2.2. Preparation of solid polymer electrolytes

All materials were stored and handled in the inert atmosphere of an Ar-filled M-Braun dry glove box (UniLab, H_2O and O_2 < 0.5 ppm). All the SPE formulations were prepared via solvent-free extrusion using a mini-compounder (Haake MiniLab II, Thermo Scientific).

The preparation procedure was previously optimized and reported [30]. The molar ratio between [EO] and [Li^+] units was fixed at 20:1, as this composition was previously identified as optimal for achieving high ionic conductivity at elevated temperatures while minimizing electrolyte stickiness. The PEO-PEC ratios selected for this study were also based on previously reported optimized compositions [30]. Thus, three electrolyte formulations were investigated: (i) PEO–PEC (1:1), (ii) PEO–PEC (1:1) encompassing SN, and (iii) PEO–PEC (7:3) encompassing SN. For SN-based systems, the SN content was based on the ratio optimized in a previous study by Xu et al. (EO:SN = 4:1) [26]. The obtained SPEs were quasi-transparent and homogeneous, and designated as SPE (namely, PEO–PEC (1:1)), SPE(1:1) + SN, and SPE(7:3) + SN, respectively. Briefly, all components were weighed and transferred into a glovebox under an inert argon atmosphere. The mixtures were subsequently processed in a mini extruder under a constant N_2 flow to avoid possible water contamination. Firstly, a portion of the PEO-PEC blend was introduced into the extruder, followed by SN and LiTFSI salt (together with 4,4′-difluorobenzophenone as a photoinitiator for crosslinkable formulations), and finally the remaining PEO-PEC fraction. The components were mixed at 120 °C and 130 rpm for 15 min to ensure homogeneous mixing and complete dissolution of all constituents. The resulting formulations were extruded as filaments, stored under vacuum, and transferred back into the glovebox. Truly SPEs were prepared by hot-pressing under an inert atmosphere at 70 °C and 25 bar, following a pre-heating step of 15 min at 70 °C, yielding membranes approximately 100 μm thick and ~10 cm in diameter. To obtain crosslinked SPEs, the same hot-pressing procedure was exploited, followed by UV-induced photopolymerization (UV-curing, UV-crosslinking) at around 70 °C for 3 min on each side under a UV Lamp (DYMAX ECE 5000 flood lamps) at 40 mW cm^2. All SPEs underwent another drying step at 40 °C under vacuum for 12 h in the B-585 oven (Buchi Glass Drying Oven, Switzerland) and then were stored in the glove box.

2.3. Characterization techniques

The optical transmittance of the SPE membranes was measured measured by Fourier transform infrared spectroscopy (FT-IR) using a spectrometer (Nicolet™ iS50 FTIR, ThermoFisher).

The thermal stability was measured by thermogravimetric analysis (TGA, Netzsch TG 209 F3), which was conducted between 25 and 600 °C under a nitrogen atmosphere, using a heating ramp of 10 °C min^{-1}. The onset weight loss temperature (T_{onset}) was determined as the point in the TGA curve at which a significant deviation from the horizontal was observed and then rounded to the nearest 5 °C.

Raman spectroscopy was carried out using a Renishaw inVia (H43662 model, Gloucestershire, UK) equipped with a near infrared laser line (785 nm) and a 50× objective with a power of 1 mW in the range between 150 and 1500 cm^{-1}.

Differential Scanning Calorimetry (DSC) analysis was performed on a Netzsch DSC 214 Polyma. Samples were hermetically sealed in Al pans inside the argon-filled glove-box (MBRAUN MB-Labstar, H_2O and O_2 content <0.5 ppm). Three heating-cooling cycles with a heating rate of 5, 5 and 3 °C min^{-1} were carried out for each sample under N_2 atmosphere. The glass transition temperature (T_g) of the different SPE was determined from the heating curve during the second heating/cooling cycle at 5 °C min^{-1} rate. The crystallization temperature (T_c) was determined from the cooling curve during the second heating/cooling cycle at 5 °C min^{-1} rate.

Dynamic mechanical thermal analysis (DMTA) was carried on a Q800 instrument (TA Instruments). Measurements were conducted using rectangular bar specimens obtained from the SPE membranes. A fixed oscillation frequency of 1 Hz was applied, and temperature was ramped from −70 to 60 °C at a rate of 3 °C min^{-1}.

2.3.1. Electrical and electrochemical characterization

The ionic conductivity of the samples was determined by electrochemical impedance spectroscopy (EIS), using a multichannel VMP3 electrochemical workstation (potentiostat/galvanostat/frequency response analyser by Biologic). A membrane disk of 16 mm in diameter, with a thickness of about 120 μm, was sandwiched between two stainless-steel (SS) blocking electrodes in an SS||SPE||SS configuration using ECC Std model electrochemical test cells (EL-CELL, Germany). For each SPE, the thickness was accurately measured before and after tests using a micrometer (Mitutoyo). EIS data were recorded on the VMP-3 electrochemical workstation in a frequency range of 0.1 Hz – 1 MHz and applying a sinusoidal voltage of 20 mV at various temperatures (20−80 °C) using an environmentally controlled climatic chamber (MK 53 E2 from BINDER, Germany). Nyquist plots were analysed using the Biologic EC-Lab® advanced software for electrochemical research. The ionic conductivity was determined according to Equation (1):

$$\sigma = D/AR \tag{1}$$

where D is the sample thickness (cm), A is the electrode area (cm^2), and R is the resistance (Ω).

The electrochemical stability at anodic voltages (oxidation) was evaluated by linear sweep voltammetry (LSV) in the range from the open circuit voltage (E_{ocv}) to 6.0 V with a scan rate of 0.1 mV s^{-1}. Test cells were assembled by simply sandwiching the materials in a Li|| SPE|| carbon-coated Al (CC-Al) configuration for LSV and connected to the VMP3 potentiostat/galvanostat for analysis. In addition, chronoamperometry (CA) measurements were conducted at stepwise potentials within the 3.5–5 V range to precisely probe the oxidative stability under constant voltage conditions.

The lithium-ion transference number (t_{Li^+}) was determined using a combination of direct current (DC) polarization and alternating current (AC) impedance methods. The AC impedance spectra before and after polarization were obtained via EIS. The transference number was calculated using Equation (2):

$$t_{Li^+} = \frac{I_s(\Delta V - I_0 R_0)}{I_0(\Delta V - I_s R_s)} \tag{2}$$

where R_0 and R_s are the impedance resistance before and after DC polarizations, respectively I_0 and I_s are the initial and final current values after polarization, respectively, and ΔV represents the applied polarization voltage (20 mV).

Lithium plating/stripping tests were performed at 40 °C in symmetrical Li||SPE||Li configuration. The rate-dependent experiment was

performed by varying the current density between 25, 50, 75, 100, and 150 μA cm^{-2} with a fixed 1h for each plating and stripping step. This measurement evaluated interfacial stability and polarization behavior under varying current densities. The SPE stability and compatibility with lithium metal were further evaluated through long-term lithium plating/stripping cycling at 25 μA cm^{-2} (fixed plated/stripped areal capacity per half cycle: 0.1 mAh cm^{-2}), aimed at assessing dendrite suppression and interfacial integrity.

The electrochemical behaviour performance of the optimized SPE under practical operating conditions was explored in laboratory-scale SSLMBs assembled in either Li||SPE||$LiFePO_4$ (LFP) or Li||SPE||$LiNi_{0.6}Mn_{0.2}Co_{0.2}O_2$ (NMC622) configurations housed in ECC-Std testing hardware (EL-CELL, Germany). Galvanostatic charge–discharge experiments were performed at 40 °C to investigate rate capability under representative working conditions. A C/10 rate corresponds to a current density of 170 mAh g^{-1}, calculated based on the mass of the active material. Cathodes were prepared via a conventional slurry-casting method. For LFP composite cathode poly(vinylidene fluoride) (PVdF) was used as binder, which was first dissolved in N-methyl-2-pyrrolidone (NMP) under continuous stirring. Separately, the active material and conductive carbon additive (Super C65) were thoroughly mixed and ground to ensure uniform dispersion. The powder mixture was subsequently added to the PVdF/NMP solution to form a homogeneous slurry with a mass composition of 80:10:10 (active material: Super C65: PVdF). Homogenization was further enhanced using a Thinky speed mixer (ARE-250 CE). The resulting slurry was coated onto aluminum foil using a doctor blade with a 300 μm gap. The electrodes were dried at 70 °C for 2 h and then further dried at room temperature. After drying, the films were punched into electrodes, and vacuum-dried overnight at 120 °C prior to cell assembly. The final active material loading ranged around 7 mg cm^{-2}. For NMC composite cathode a mixture of PEC/PMLiTFSI (9:1) was used as binder. The cathode was obtained following the same preparation procedure used above and the final composition was of 70:20:10 (NMC622:PEC/PMLiTFSI:Super C65). After drying the final active material loading was in the range of 4 mg cm^{-2}.

3. Results and discussion

Fig. 1a shows a photograph of the SPE(1:1) + SN membrane, which appears quasi-transparent, homogeneous, elastic, and self-standing, indicating its suitability for subsequent structural and electrochemical characterization. The effect of UV exposure on SN was investigated using FT-IR spectroscopy. Fig. 1b shows the FT-IR spectra of pristine SN and the SPE(1:1) + SN electrolyte before UV exposure, after 1 min of irradiation, and after 3 min of irradiation. The SN-containing SPE was exposed to UV light under the same conditions employed for electrolyte preparation. As shown in Fig. 1b, the characteristic absorption band at 2252 cm^{-1}, assigned to the cyano (C ≡ N) stretching vibration, remains essentially unchanged even after 3 min of UV exposure. This observation indicates that the cyano functional groups of SN are largely preserved during the UV-curing process, confirming the chemical stability of SN under the applied irradiation conditions.

The Raman spectrum of PEO (Fig. S1a) is characterized by several active vibrational modes associated with the polymer backbone and ether functionalities including τ_{COC} 1280 and 1480 cm^{-1}, symmetric and asymmetric ν_{COC} 1060–1130 cm^{-1} and ρ_{COC} and ν_{CC} around 840–865 cm^{-1} [31]. Blending with PEC (orange line) induced the presence of massively broad bands of ν_{CH} 1300-1400 cm^{-1}, ν_{CO} 1140 cm^{-1}, σ_{COC} at 800 cm^{-1} and σ_{OCO} at 740 cm^{-1}, respectively. Encompassing SN plasticizer induced the appearance of several characteristic bands around 500 cm^{-1} due to $\sigma_{C\text{-}CN}$ and $\sigma_{C\text{-}C\text{-}C}$ (Fig. S1b) [32]. The prominent band in Fig. S1c at 740 cm^{-1} has been reported to be due to $TSFI^-$ anion. This peak is slightly shifted to lower wavenumber, which has been reported due to the different environment for the $TSFI^-$ anion. Due to the weak interaction of the anion with PEO, the perturbation of the S–N stretching mode can be due to anion–cation association [31]. Finally, the different ratio of PEO/PEC did not induce any appreciable difference in signals. As shown in Fig. S1d, the Raman spectrum in the range of 720–760 cm^{-1} indicates the dissociation state of TFSI. The fitting results suggest that the SPE (7:3) and (1:1) + SN samples exhibit a higher solvent separated ion pair (SSIP) structure and a decrease in free $TFSI^-$ions compared to that of the sample without SN; thus, a high proportion of lithium salts dissociated in the electrolyte [33].

To investigate the thermal properties and crystallinity of the SPEs, DSC measurements were performed. This aspect is especially crucial in PEO-based electrolytes, where ionic transport is predominantly associated with the amorphous phase and its segmental dynamics, while the crystalline fraction generally acts as a barrier to chain relaxation and Li^+ migration. Hence, reducing PEO crystallinity and promoting a larger amorphous fraction are essential to improve ionic conductivity, particularly at ambient temperature [34]. Fig. 2a shows the DSC thermograms of PEO/LiTFSI, SPE(1:1) + SN, and SPE(7:3) + SN. The PEO/LiTFSI SPE reveals a characteristic endothermic transition at −32 °C, attributed to a solid-solid transition from crystallinity to the plastic crystalline phase, along with a melting peak at around 60 °C. As reported in a previous work, this SPE has a semi-crystalline nature, with a crystallinity degree of approximately 33% [30]. In contrast, no distinct melting or crystallization peaks are observed for the SN-based SPEs, indicating a predominantly amorphous structure. Actually, the incorporation of PEC disrupts the formation of crystalline domains in PEO, while UV-induced crosslinking generates a network structure that further suppresses PEO recrystallization [35]. Both SN-based SPEs show two glass transition temperatures (T_g), located at −50 °C (PEO-rich phase) and −10 °C

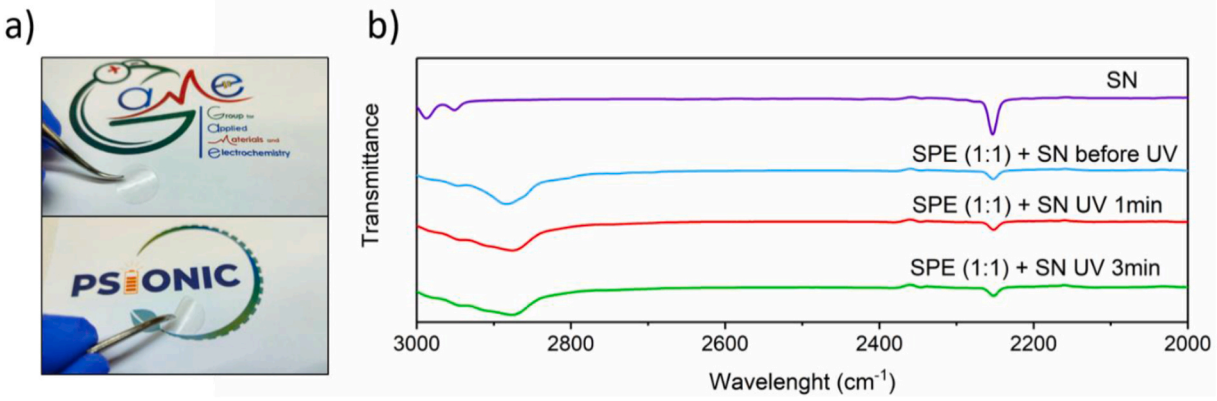

Fig. 1. a) Digital photograph of the self-standing, flexible, and quasi-transparent SPE(1:1) + SN membrane. b) FT-IR spectra of pristine SN and the SPE(1:1) + SN electrolyte recorded before UV exposure and after 1 and 3 min of UV irradiation, respectively.

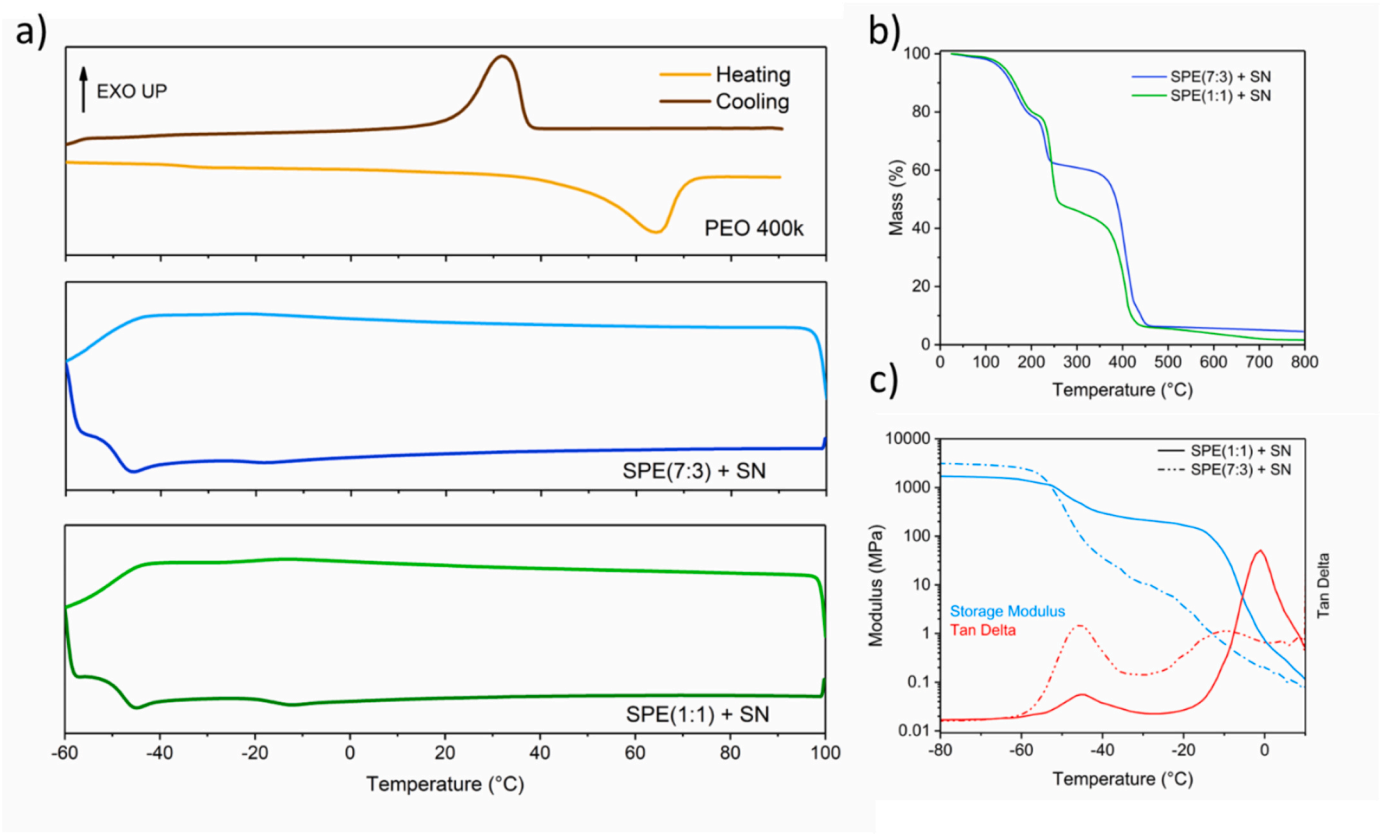

Fig. 2. Thermal characteristics of the SPE under study: a) DSC thermograms of PEO/LiTFSI, SPE(1:1) + SN, and SPE(7:3) + SN recorded at a heating rate of 1 °C min^{-1}; b) TGA profiles obtained under N_2 atmosphere at a heating rate of 10 °C min^{-1}; c) DMA profiles of SPE(1:1) + SN and SPE(7:3) + SN.

(PEC-rich phase), indicating at least partial phase separation between the two polymer components. Compared SPE non encompassing SN (Fig. S2–3), both T_g values decrease by approximately 20–30 °C. This behaviour is attributed to the plasticizing effect of SN, which increases free volume and enhances polymer chain mobility [36].

TGA analysis was carried out in the temperature range of 25–800 °C to evaluate the thermal stability of the SN-containing SPEs, as shown in Fig. 2b. The SPEs exhibit thermal stability up to around 136 °C, corresponding to 5% weight loss, while the SN-free SPE shows the onset of degradation over 200 °C (Fig. S4). The initial weight loss observed at around 130 °C can be attributed to sublimation of SN [37]. Nevertheless, the $T_{95\%}$ of 136 °C for the plasticized SPEs confirm their adequate thermal robustness for operation under moderately high temperatures in practical applications. Moreover, this result indicates that the extrusion process at ~120 °C did not induce chemical degradation of the polymer matrix. TGA curves of both SN-SPE formulations reveal three distinct weight-loss stages. The initial mass loss observed between 130 and 220 °C is mainly attributed to the evaporation of SN. Above 220 °C, degradation of the aliphatic polycarbonate chains begins. The final weight-loss stage, occurring above 350 °C, is associated to the decomposition of the PEO polymer backbone and its complexes with LiTFSI. Typically, salt-doped PEO systems exhibit a two-step decomposition behaviour: the first step, occurring around 380 °C, corresponds to polymer chain scission, while the second decomposition event at approximately 430 °C is related to the breakdown of LiTFSI ethylene oxide coordination complexes [38].

DMA was performed to evaluate the mechanical behaviour of the plasticized SPEs. The measurements reveal a reduction in the T_g and further confirm the partial immiscibility between the PEO and PEC phases (Fig. 2c). The Tan Delta curve exhibits two distinct α-relaxation peaks for both SPEs, corresponding to the glass transitions of the individual PEO-rich and PEC-rich domains. These T_gs are approximately 20 °C lower than those observed for plasticer-free systems (−30 °C and +20 °C, respectively [39]), demonstrating the effective plasticizing effect of SN, which promotes increased chain mobility and softening of both polymer phases (Fig. S5).

The temperature dependence of the ionic conductivity for the investigated SPEs is shown in Fig. 3a. SPE(7:3) + SN exhibits slightly higher ionic conductivity across the entire temperature range, reaching values of 2×10^{-4} and 3.2×10^{-5} S cm^{-1} at 70 and 40 °C respectively. This enhancement can be directly attributed to the plasticizing effect of SN, which reduces T_g, suppresses residual crystallinity, and increases the free volume within the polymer matrix. These combined effects promote enhanced segmental chain mobility, thereby facilitating Li^+ transport [26]. A comparison between the two SN-containing systems further highlights the critical role of polymer composition. The SPE(7:3) + SN electrolyte consistently outperforms the corresponding 1:1 formulation that at 40 °C shows a conductivity of 3.2×10^{-5} S cm^{-1}, indicating that the higher PEO fraction provides a greater density of ether oxygen coordination sites for Li^+ migration. Meanwhile, PEC and SN synergistically inhibit PEO recrystallization, preserving an amorphous structure favorable for efficient ionic conduction.

The ESW of the investigated SPEs is a critical parameter for practical application, as it determines compatibility with high-voltage cathode materials and enables the development of high-energy-density lithium-based batteries. Fig. 3b shows the oxidative (anodic) stability of the SN-containing SPEs, assessed through chronoamperometry (CA) by monitoring the current response during a stepwise potential sweep from 3 V to 5 V vs. Li^+/Li at 40 °C. Each voltage step produces an initial current spike followed by a gradual decay toward a quasi-steady-state value with no significant current flow for the investigated electrolytes up to 4.9 vs. Li^+/Li, which can meet the requirement of typical high-energy 4V class cathode materials. Using a threshold of ~5 μA cm^{-2}, no significant current increase is observed for the SN-containing SPEs up to 4.8 V vs.

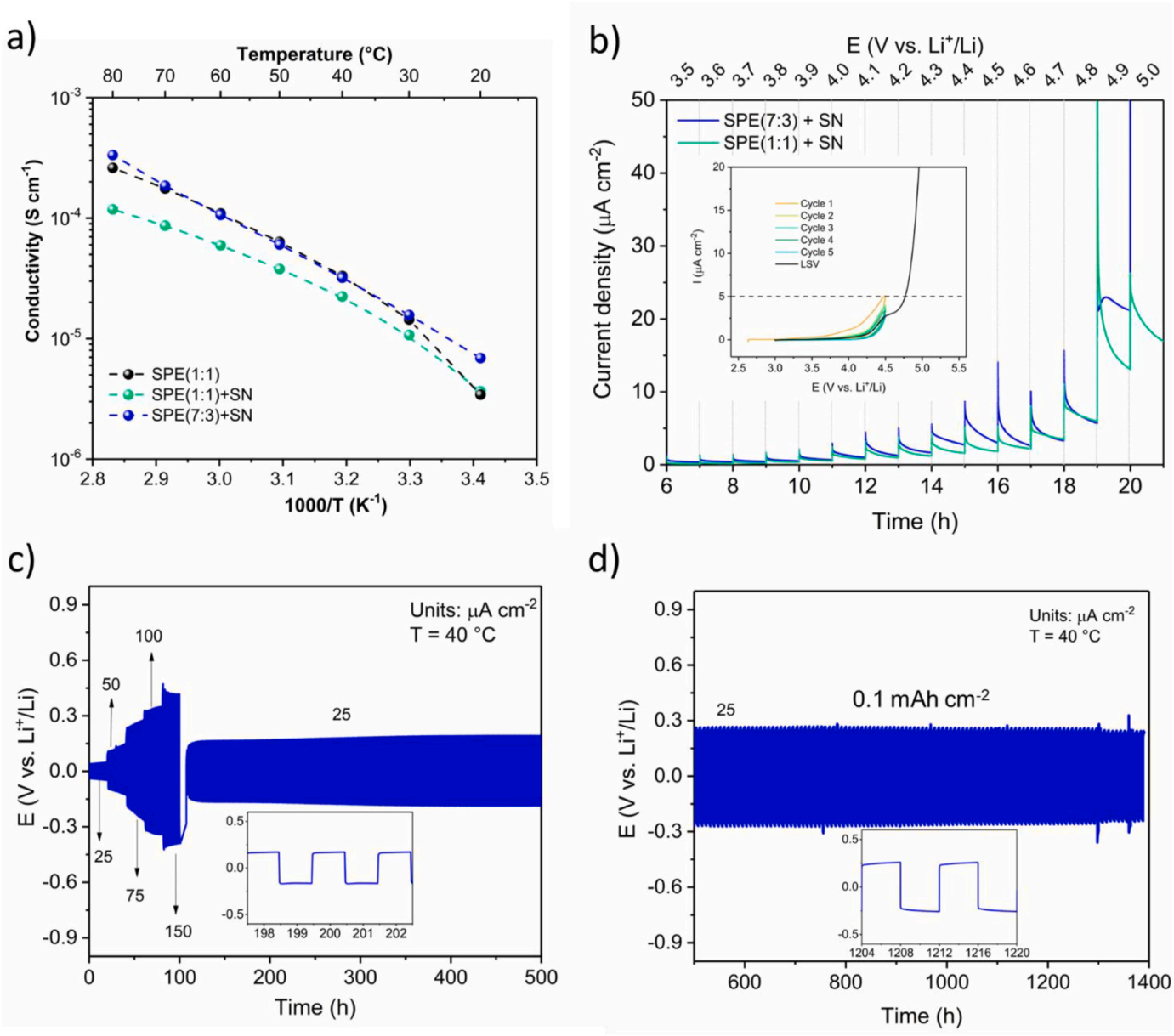

Fig. 3. a) Arrhenius plots of ionic conductivity vs. inverse temperature of SPEs under study. b) CA of SN-containing SPEs using a Li/SPE/Al-CC cell during stepwise anodic polarization at 40 °C; inset: LSV profile of SPE(7:3) + SN at 40 °C (scan rate of 0.1 mV s^{-1}). c) Galvanostatic lithium plating/stripping cycling in symmetric Li||Li cells employing SPE(7:3) + SN at current densities ranging from 25 to 150 µA cm^{-2}. d) Long-term lithium plating/stripping test of SPE(7:3) + SN at 25 µA cm^{-2} (T = 40 °C).

Li^+/Li, which is notably higher than that of the pristine SPE [39]. In the SPE system under study, the incorporation of PEC increases the fraction of carbonate functionalities, which possess intrinsically higher anodic stability than ether-based PEO segments, thus chiefly contributing to delaying detectable oxidation (anodic) currents [40,41]. In addition, also the addition of SN is effective in this respect, as it exhibits a wide electrochemical stability window and has previously been reported to remain stable above 5 V vs. Li^+/Li in solid-state electrolyte systems [42]. Moreover, the LSV profile included as inset of Fig. 3b for SPE(7:3) + SN, shows the onset of a current increase at approximately 4.8 V, in good agreement with the behavior observed in the CA. At the same time, we observe no distinct sign of redox features attributable to SN during the scan, excluding the potential hazards of cyanide formation in practical applications [43]. Notably, the PEO–PEC (1:1) composition exhibits slightly lower anodic current densities compared to the 7:3 formulation, which can be attributed to its higher PEC fraction [44]. This enhanced oxidative stability exceeds that of the pristine SPE and satisfies the operational requirements of typical high-energy 4V-class layered oxide cathode materials.

As for their enhanced electrical and electrochemical characteristics, SN-added SPEs were selected for further galvanostatic testing in both symmetric Li||Li and Li-metal laboratory-scale cells. Fig. 3c and d show the lithium plating/stripping behavior of SPE(7:3) + SN evaluated at 40 °C under various current densities ranging from 25 to 150 µA cm^{-2}, as well as during long-term cycling at 25 µA cm^{-2} (for this latter part of the test, after 500h the areal plated/stripped capacity was increased to 0.1 mAh cm-2). The SPE exhibits low polarization across different current densities, with an overpotential of 0.4 V at the highest tested current density of 150 µA cm^{-2}. An initial gradual increase in overpotential is observed within the first few hundred hours, which is attributed to the progressive formation of a stable solid electrolyte interphase (SEI) layer at the lithium surface. SN may undergo partial reduction of nitrile

groups upon direct contact with lithium metal, leading to the formation of electronically insulating interphase species [45]. However, in the present system this decomposition appears to remain limited and self-passivating, as demonstrated by the stabilization of the overpotential during long-term, reversible galvanostatic Li plating/stripping cycling. Once a uniform and ionically conductive SEI is established, the overpotential reaches a steady-state value and remains nearly constant over 1400 h of continuous cycling, demonstrating highly stable interfacial behavior and effective suppression of dendritic growth. In contrast, the SPE (1:1) + SN (Fig. S8) exhibits a progressive increase in overpotential even at the lowest applied current density (25 μA cm^{-2}), followed by pronounced voltage polarization upon increasing the current density and eventual short-circuit failure. The lower interfacial stability of SPE(1:1) + SN at 40 °C can be attributed to its higher PEC content and comparatively lower ionic conductivity at this temperature. The reduced ionic conductivity limits efficient Li^+ transport across the interface, leading to increased local polarization and inhomogeneous lithium deposition. Such conditions, promoting uneven current distribution and enhancing the likelihood of parasitic interfacial reactions, can be attributed to the intrinsic chemical reactivity of PEC and SN toward lithium metal [46]. Similarly, SN upon contact with Li metal SN can undergo partial reduction of the nitrile groups, producing electronically insulating but ionically heterogeneous decomposition products [25]. SPE(7:3) + SN benefits from both a higher PEO fraction and the synergistic plasticizing effect of SN, resulting in improved ionic conductivity at 40 °C, enabling efficient Li^+ mobility under moderate operating conditions. Indeed, the increased PEO content provides a greater density of ether oxygen coordination sites for Li^+ transport, while SN enhances segmental mobility by reducing the T_g and suppressing residual crystallinity. Consequently, more homogeneous lithium plating/stripping is achieved, promoting the formation of a stable and ionically conductive SEI. These combined factors account for the superior interfacial stability and long-term cycling performance observed for the SPE(7:3) + SN electrolyte.

Laboratory-scale all-solid-state Li-metal cells were assembled to evaluate the electrochemical performance of the optimized SPE in combination with both medium- and high-voltage cathode materials, *viz.* LFP and NMC622, respectively. Fig. 4a shows the rate capability of the Li‖SPE(7:3) + SN‖LFP cell cycled at 40 °C at progressively increasing C-rates from C/40 to C/5. At low current regime (C/40), the cell delivers a high specific discharge capacity of 157 mAh g^{-1}, which corresponds to full practical capacity and close to the theoretical capacity of the commercial LFP used as cathode active material (the LFP composite cathode was prepared by standard slurry casting with PVdF binder). Upon increasing the rate, the cell maintains capacities of 147 and 135 mAh g^{-1} at C/15 and C/10, respectively. The relatively small capacity decay demonstrates that the SPE(7:3) + SN electrolyte provides sufficient ionic conductivity and low interfacial resistance to sustain operation even at practical current densities. This performance is superior to that observed for the pristine electrolyte, which exhibited a considerable capacity drop under similar conditions (Fig. S9). At C/5, a more pronounced capacity drop to 94 mAh g^{-1} is observed, which can be attributed to increased polarization arising from kinetic limitations typical of solid-state systems. Nevertheless, when the current density is reduced back to C/15, the discharge capacity largely recovers, confirming the absence of significant irreversible degradation. The initial Coulombic efficiency (CE) is ~98%; it soon stabilises at ~99.2% (C/20), then further improves, reaching values as high as 99.7% upon returning to C/15 in the subsequent cycles. The representative galvanostatic charge-discharge profiles at different C-rates (Fig. 4b) show that voltage polarization remains low up to C/10, increasing only slightly at current regimes as high as C/5, as expected for SPEs. It accounts for efficient charge transfer enabled by good interfacial contact between the SPE and the active material at low and intermediate rates. Nevertheless, no abnormal voltage profiles are observed, indicating homogeneous Li^+ transport, excellent active materials use, compatibility and stable interfacial behavior.

To further verify the feasibility of the SN-containing SPEs for practical applications, they were assembled in Li-metal battery cells with high-energy 4V-class mixed transition metal layered oxide cathode and lithium metal anode and cycled between 3.0 and 4.2 V vs. Li^+/Li at 40 °C (Fig. 5). The NMC622 composite cathode tape was obtained in an integrated catholyte-electrolyte form using PEO + single-ion conducting polymer active binder to enhance ionic diffusion/transport and extend anodic stability. As shown in Fig. 5a, the cell assembled with SPE(7:3) + SN delivers a reversible discharge capacity of approximately 145 mAh g^{-1} at C/15, demonstrating that the electrolyte can operate stably under oxidative potentials exceeding 4.0 V vs. Li^+/Li. Upon increasing the current density to C/10 and C/5, a gradual decrease in capacity is observed, which is primarily associated with increased polarization rather than electrolyte degradation [47]. This interpretation is supported by the recovery of the capacity when the current density is returned to C/15. The voltage profiles shown in Fig. 5b exhibit smooth and sloping charge–discharge curves typical of layered NMC cathodes.

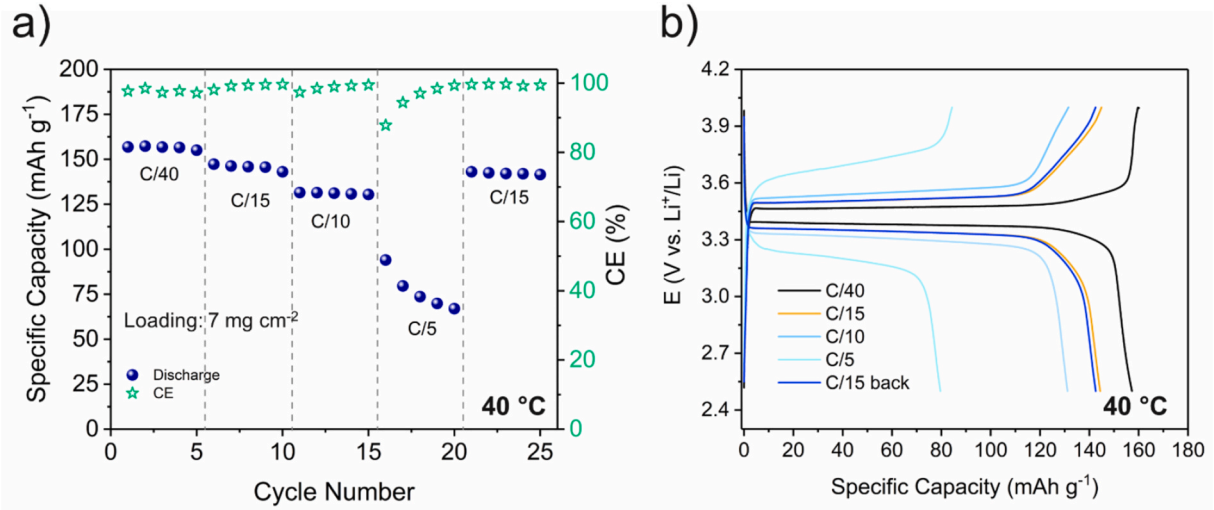

Fig. 4. Electrochemical galvanostatic charge/discharge cycling behaviour in Li‖SPE(7:3) + SN‖ $LiFePO_4$ cells: (a) rate capability evaluated at increasingly higher C-rates ranging from C/40 to C/5; (b) representative charge/discharge voltage vs. specific capacity profiles at the different C-rates. All tests were performed within a voltage window of 2.5 and 4.0 V at T = 40 °C.

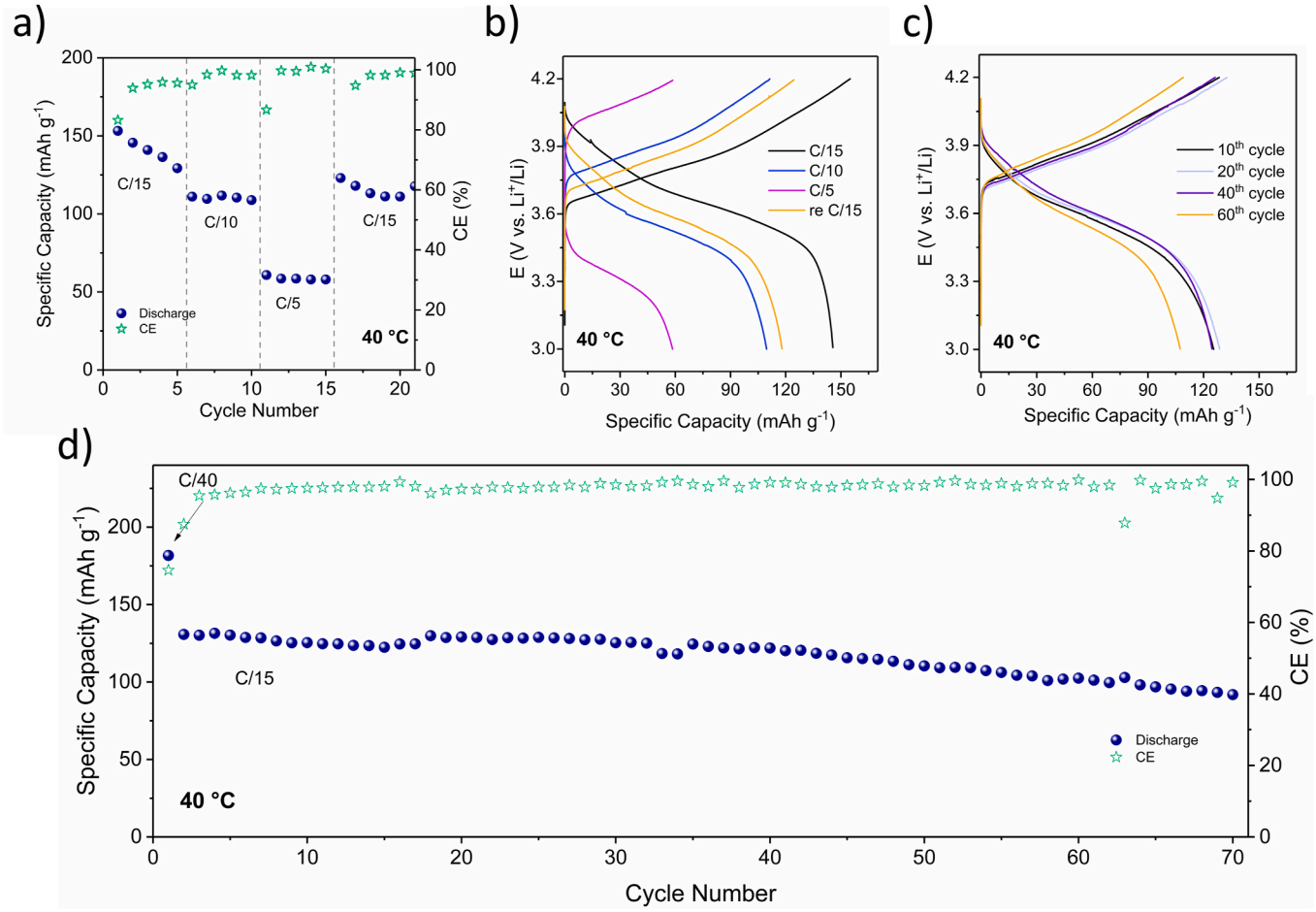

Fig. 5. Electrochemical galvanostatic charge/discharge cycling behaviour of Li‖ SPE(7:3) + SN‖NMC622 cells: (a) rate capability evaluated at C-rates ranging from C/15 to C/5; (b) representative charge/discharge voltage vs. specific capacity profiles at increasingly higher C-rates; (c) representative charge/discharge voltage vs. specific capacity profiles at C/15; (d) long-term cycling (specific capacity vs. cycle number) at C/15. All tests were performed within a voltage range of 3 and 4.2 V at T = 40 °C.

At lower current densities, the profiles display limited polarization and good reversibility, whereas higher rates lead to increased overpotential, particularly near the upper cut-off voltage. Remarkably, no abrupt voltage drops or indications of parasitic oxidation are observed, suggesting that the presence of SN and PEC improves the oxidative stability of the electrolyte. Nevertheless, the synergistic effect of the use of PEC and SN is clear; indeed, pristine SPE, both at 40 and 70 °C, was found to operate reliably only with the LFP cathode and not with high-energy NMC cathodes. For comparison, a Li‖NMC622 cell employing the SPE (1:1) + SN membrane was also assembled (Fig. S10). In this case, the cell exhibits significantly lower performance. An initial discharge capacity of ~120 mAh g^{-1} is achieved at C/15, followed by rapid capacity fading and pronounced polarization at higher current densities, with only partial recovery when returning to lower rates. The higher PEC content in the 1:1 SPE likely results in insufficient ion transport and reduced interfacial stability at high voltages, ultimately preventing sustained operation with NMC cathodes.

Long-term cycling stability of the Li-metal battery cell assembled with SPE(7:3) + SN at C/15 is shown in Fig. 5c and d. The cell maintains a stable discharge capacity over prolonged cycling, with only gradual and limited capacity fading. The corresponding CE remains in the range of 98-99% throughout the test, indicating highly reversible lithium insertion and extraction processes. Selected voltage profiles collected at different cycle numbers overlap closely, confirming that polarization does not significantly increase upon cycling and that the electrode–electrolyte interfaces remain stable over time. The successful operation of the SPE with both $LiFePO_4$ and high-voltage NMC622 cathodes at 40 °C, together with the stable cycling behavior and limited polarization growth, indicates good interfacial compatibility with both lithium metal and cathode materials under the investigated conditions.

A comparison with state-of-the-art SN-based SPEs is reported in the Supporting Information (Table S1) to contextualize the present electrolyte performance. Although higher conductivities are reported in some cases, they often rely on liquid additives/plasticizers or costly ceramic fillers such as LLZO/LLZTO. Here, a truly solid-state SPE is obtained by solvent-free extrusion/UV-curing, offering a well balanced compromise between performance, sustainability, cost, and scalability.

4. Conclusion

In this work, a solvent-free route combining melt extrusion and UV curing was developed to prepare PEO-PEC solid polymer electrolytes plasticized with succinonitrile (SN). The results show that the electrolyte performance is governed by the interplay between polymer composition and plasticization: SN lowers the glass transition temperature and supports PEC in suppressing crystallinity, thereby promoting segmental mobility and Li-ion transport, while the PEO/PEC ratio controls the balance between ionic conductivity, electrochemical stability, and interfacial compatibility with lithium metal. Within the investigated compositions, the PEO-rich SPE(7:3) + SN formulation provided the most favorable overall response, delivering an ionic conductivity of 3.2 × 10^{-5} S cm^{-1} at 40 °C and an anodic stability up to about 4.8 V vs. Li^+/

Li.

This optimized SPE also exhibited stable Li plating/stripping in symmetric Li||Li cells for more than 1400 h at 40 °C, with moderate and stabilized polarization, indicating improved interfacial stability towards lithium metal. The practical relevance of this electrolyte was further demonstrated in all-solid-state Li-metal cells with both $LiFePO_4$ and high-energy 4V-class NMC622 cathodes. In particular, SPE(7:3) + SN enabled discharge capacities close to the practical values of the active materials, namely ~157 mAh g^{-1} for LFP and ~145 mAh g^{-1} for NMC622, while maintaining stable cycling at 40 °C and compatibility with practical operation up to 4.2 V.

Overall, this work shows that the integration of dry extrusion, UV-induced crosslinking of PEO-PEC polymer networks, and SN plasticization provides an effective route to overcome key limitations of conventional PEO-based SPEs. Beyond the specific crosslinked PEO-PEC/SN systems investigated here, solvent-free manufacturing emerges as a promising and scalable platform for developing mechanically compliant and electrochemically stable polymer-based electrolytes for next-generation high-energy density solid-state Li-metal batteries.

CRediT authorship contribution statement

Francesco Gambino: Data curation, Investigation, Methodology, Validation, Visualization, Writing – original draft. **Hamideh Darjazi:** Investigation, Methodology, Validation, Visualization, Writing – review & editing. **Giuseppe Antonio Elia:** Supervision, Validation, Writing – review & editing. **Claudio Gerbaldi:** Funding acquisition, Supervision, Writing – review & editing.

Declaration of competing interest

The authors declare that they have no known competing financial interests or personal relationships that could have appeared to influence the work reported in this paper.

Acknowledgements

The PSIONIC project has received funding from the European Union's Horizon Europe Research and Innovation Programme under Grant Agreement N. 101069703. Part of this study was carried out within the "Enabling high-energy, room temperature all solid-state lithium metal batteries with advanced polymer-based electrolytes and high-voltage cathodes through enhanced interface control (EnabLi)" project, funded by the Italian Ministero dell'Università e della Ricerca (MUR) within the PRIN 2022 program (D.D. 104 - 02/02/2022). The manuscript reflects only the authors' views and opinions, neither the European Union nor the European Commission can be considered responsible for them. Support under the MUR program "Dipartimenti di Eccellenza 2023–2027" (CUP E17G22001490006) is gratefully acknowledged.

Appendix A. Supplementary data

Supplementary data to this article can be found online at https://doi.org/10.1016/j.jpowsour.2026.240803.

Data availability

Data will be made available on request.

References

[1] A. Manthiram, X. Yu, S. Wang, Lithium battery chemistries enabled by solid-state electrolytes, Nat. Rev. Mater. 2 (2017) 16103.
[2] M. Armand, J.-M. Tarascon, Building Better Batteries, Nature 451 (2008) 652–657, https://doi.org/10.1038/451652a.
[3] B. Liu, J.-G. Zhang, W. Xu, Advancing lithium metal batteries, Joule 2 (2018) 833–845, https://doi.org/10.1016/j.joule.2018.03.008.
[4] K. Takada, Progress in solid electrolytes toward realizing solid-state lithium batteries, J. Power Sources 394 (2018) 74–85, https://doi.org/10.1016/j.jpowsour.2018.05.003.
[5] H. Wan, S. Liu, T. Deng, J. Xu, J. Zhang, X. He, X. Ji, X. Yao, C. Wang, Bifunctional interphase-enabled Li_{10} GeP_2 S_{12} electrolytes for lithium–sulfur battery, ACS Energy Lett. 6 (2021) 862–868, https://doi.org/10.1021/acsenergylett.0c02617.
[6] M. Henriksen, K. Vaagsaether, J. Lundberg, S. Forseth, D. Bjerketvedt, Explosion characteristics for Li-ion battery electrolytes at elevated temperatures, J. Hazard. Mater. 371 (2019) 1–7, https://doi.org/10.1016/j.jhazmat.2019.02.108.
[7] W.-P. Chen, H. Duan, J.-L. Shi, Y. Qian, J. Wan, X.-D. Zhang, H. Sheng, B. Guan, R. Wen, Y.-X. Yin, S. Xin, Y.-G. Guo, L.-J. Wan, Bridging interparticle Li^+ conduction in a soft ceramic oxide electrolyte, J. Am. Chem. Soc. 143 (2021) 5717–5726, https://doi.org/10.1021/jacs.0c12965.
[8] N. Wu, P. Chien, Y. Qian, Y. Li, H. Xu, N.S. Grundish, B. Xu, H. Jin, Y. Hu, G. Yu, J. B. Goodenough, Enhanced surface interactions enable fast Li^+ conduction in oxide/polymer composite electrolyte, Angew. Chem. Int. Ed. 59 (2020) 4131–4137, https://doi.org/10.1002/anie.201914478.
[9] G.B. Appetecchi, F. Croce, G. Dautzenberg, M. Mastragostino, F. Ronci, B. Scrosati, F. Soavi, A. Zanelli, F. Alessandrini, P.P. Prosini, Composite polymer electrolytes with improved lithium metal electrode interfacial properties: I. Elechtrochemical properties of dry PEO-LiX systems, J. Electrochem. Soc. 145 (1998) 4126–4132, https://doi.org/10.1149/1.1838925.
[10] R. Fang, B. Xu, N.S. Grundish, Y. Xia, Y. Li, C. Lu, Y. Liu, N. Wu, J.B. Goodenough, Li_2S_6-Integrated PEO-based polymer electrolytes for all-solid-state lithium-metal batteries, Angew. Chem. Int. Ed. 60 (2021) 17701–17706, https://doi.org/10.1002/anie.202106039.
[11] J.L. Olmedo-Martínez, L. Porcarelli, G. Guzmán-González, I. Calafel, M. Forsyth, D. Mecerreyes, A.J. Müller, Ternary Poly(ethylene oxide)/Poly(l , l -lactide) PEO/PLA blends as high-temperature solid polymer electrolytes for lithium batteries, ACS Appl. Polym. Mater. 3 (2021) 6326–6337, https://doi.org/10.1021/acsapm.1c01093.
[12] D. Zhou, D. Shanmukaraj, A. Tkacheva, M. Armand, G. Wang, Polymer electrolytes for lithium-based batteries: advances and prospects, Chem 5 (2019) 2326–2352, https://doi.org/10.1016/j.chempr.2019.05.009.
[13] G. Homann, L. Stolz, J. Nair, I.C. Laskovic, M. Winter, J. Kasnatscheew, Poly (Ethylene oxide)-based electrolyte for solid-state-lithium-batteries with high voltage positive electrodes: evaluating the role of electrolyte oxidation in rapid cell failure, Sci. Rep. 10 (2020) 4390, https://doi.org/10.1038/s41598-020-61373-9.
[14] M. Zhu, J. Ma, Z. Wang, H. He, X. Yao, In-situ polymerized gel polymer electrolytes for stable solid-state lithium batteries with long-cycle life, J. Power Sources 585 (2023) 233651, https://doi.org/10.1016/j.jpowsour.2023.233651.
[15] L. Porcarelli, P. Sutton, V. Bocharova, R.H. Aguirresarobe, H. Zhu, N. Goujon, J. R. Leiza, A. Sokolov, M. Forsyth, D. Mecerreyes, Single-Ion conducting polymer nanoparticles as functional fillers for solid electrolytes in lithium metal batteries, ACS Appl. Mater. Interfaces 13 (2021) 54354–54362, https://doi.org/10.1021/acsami.1c15771.
[16] H. Wu, Y. Cao, H. Su, C. Wang, Tough gel electrolyte using double polymer network design for the safe, stable cycling of lithium metal anode, Angew. Chem. Int. Ed. 57 (2018) 1361–1365, https://doi.org/10.1002/anie.201709774.
[17] J. Deng, W. Yang, Y. Zhang, L. Pan, F. Kang, X. Ji, H. Wu, Combustion characteristics and fire risk assessment of EC/DMC/EMC electrolytes for Li-ion batteries, J. Energy Storage 110 (2025) 115308, https://doi.org/10.1016/j.est.2025.115308.
[18] S. Ferrari, M. Falco, A.B. Muñoz-García, M. Bonomo, S. Brutti, M. Pavone, C. Gerbaldi, Solid-State post Li metal ion batteries A sustainable forthcoming reality, Adv. Energy Mater. 11 (2021) 2100785.
[19] Y. Ren, S. Chen, M. Odziomek, J. Guo, P. Xu, H. Xie, Z. Tian, M. Antonietti, T. Liu, Mixing functionality in polymer electrolytes: a new horizon for achieving high-performance all-solid-state lithium metal batteries, Angew. Chem. Int. Ed. 64 (2025) e202422169, https://doi.org/10.1002/anie.202422169.
[20] P.-J. Alarco, Y. Abu-Lebdeh, A. Abouimrane, M. Armand, The plastic-crystalline phase of succinonitrile as a universal matrix for solid-state ionic conductors, Nat. Mater. 3 (2004) 476–481, https://doi.org/10.1038/nmat1158.
[21] L.-Z. Fan, Y.-S. Hu, A.J. Bhattacharyya, J. Maier, Succinonitrile as a versatile additive for polymer electrolytes, Adv. Funct. Mater. 17 (2007) 2800–2807, https://doi.org/10.1002/adfm.200601070.
[22] F. Chen, W. Zha, D. Yang, S. Cao, Q. Shen, L. Zhang, D.R. Sadoway, All-solid-state lithium battery fitted with polymer electrolyte enhanced by solid plasticizer and conductive ceramic filler, J. Electrochem. Soc. 165 (2018) A3558–A3565, https://doi.org/10.1149/2.1371814jes.
[23] V. Van Laack, F. Langer, A. Hartwig, K. Koschek, Succinonitrile-polymer composite electrolytes for Li-Ion solid-state batteries—the influence of polymer additives on thermomechanical and electrochemical properties, ACS Omega 8 (2023) 9058–9066, https://doi.org/10.1021/acsomega.2c02174.
[24] W. Zha, J. Li, W. Li, C. Sun, Z. Wen, Anchoring succinonitrile by solvent-Li+ associations for high-performance solid-state lithium battery, Chem. Eng. J. 406 (2021) 126754, https://doi.org/10.1016/j.cej.2020.126754.
[25] Y. Liu, Y. Zhao, W. Lu, L. Sun, L. Lin, M. Zheng, X. Sun, H. Xie, PEO based polymer in plastic crystal electrolytes for room temperature high-voltage lithium metal batteries, Nano Energy 88 (2021) 106205, https://doi.org/10.1016/j.nanoen.2021.106205.
[26] S. Xu, Z. Sun, C. Sun, F. Li, K. Chen, Z. Zhang, G. Hou, H. Cheng, F. Li, Homogeneous and fast ion conduction of PEO-Based solid-state electrolyte at low

temperature, Adv. Funct. Mater. 30 (2020) 2007172, https://doi.org/10.1002/adfm.202007172.
[27] B. Chen, Z. Huang, X. Chen, Y. Zhao, Q. Xu, P. Long, S. Chen, X. Xu, A new composite solid electrolyte PEO/Li10GeP2S12/SN for all-solid-state lithium battery, Electrochim. Acta 210 (2016) 905–914, https://doi.org/10.1016/j.electacta.2016.06.025.
[28] M. Falco, C. Simari, C. Ferrara, J.R. Nair, G. Meligrana, F. Bella, I. Nicotera, P. Mustarelli, M. Winter, C. Gerbaldi, Understanding the effect of UV-Induced cross-linking on the physicochemical properties of highly performing PEO/LiTFSI-Based polymer electrolytes, Langmuir 35 (2019) 8210–8219, https://doi.org/10.1021/acs.langmuir.9b00041.
[29] D.F. Miranda, C. Versek, M.T. Tuominen, T.P. Russell, J.J. Watkins, Cross-linked block copolymer/ionic liquid self-assembled blends for polymer gel electrolytes with high ionic conductivity and mechanical strength, Macromolecules 46 (2013) 9313–9323, https://doi.org/10.1021/ma401302r.
[30] F. Gambino, M. Gastaldi, A. Jouhara, S. Malburet, S. Galliano, N. Cavallini, G. Colucci, M. Zanetti, A. Fina, G.A. Elia, C. Gerbaldi, Formulating PEO-polycarbonate blends as solid polymer electrolytes by solvent-free extrusion, J. Power Sources Adv 30 (2024) 100160, https://doi.org/10.1016/j.powera.2024.100160.
[31] I. Rey, J.C. Lassègues, J. Grondin, L. Servant, Infrared and Raman study of the PEO-LiTFSI polymer electrolyte, Electrochim. Acta 43 (1998) 1505–1510, https://doi.org/10.1016/S0013-4686(97)10092-5.
[32] C. Xin, K. Wen, C. Xue, S. Wang, Y. Liang, X. Wu, L. Li, C. Nan, Composite cathodes with succinonitrile-based ionic conductors for long-cycle-life solid-state lithium metal batteries, Batter. Supercaps 5 (2022) e202100162, https://doi.org/10.1002/batt.202100162.
[33] Y.-W. Song, H. Lee, S. Park, S.-J. Park, M.-Y. Kim, C. Yun, J. Kim, J. Lim, Succinonitrile coordination-induced in situ polymerization-based composite solid electrolytes for solid-state batteries, J. Power Sources 656 (2025) 237924, https://doi.org/10.1016/j.jpowsour.2025.237924.
[34] Z. Xue, D. He, X. Xie, Poly(ethylene oxide)-based electrolytes for lithium-ion batteries, J. Mater. Chem. A 3 (2015) 19218–19253, https://doi.org/10.1039/C5TA03471J.
[35] L. Porcarelli, C. Gerbaldi, F. Bella, J.R. Nair, Super soft all-ethylene oxide polymer electrolyte for safe all-solid lithium batteries, Sci. Rep. 6 (2016) 19892, https://doi.org/10.1038/srep19892.
[36] Z. Yang, Y. Luo, R. Wang, High-safety all-solid-state lithium-ion battery working at ambient temperature with in situ UV-Curing polymer electrolyte on the electrode, Chemelectrochem 7 (2020) 2599–2607, https://doi.org/10.1002/celc.202000411.
[37] R. He, M. Echeverri, D. Ward, Y. Zhu, T. Kyu, Highly conductive solvent-free polymer electrolyte membrane for lithium-ion batteries: effect of prepolymer molecular weight, J. Membr. Sci. 498 (2016) 208–217, https://doi.org/10.1016/j.memsci.2015.10.008.
[38] H. Beyer, S. Meini, N. Tsiouvaras, M. Piana, H.A. Gasteiger, Thermal and electrochemical decomposition of lithium peroxide in non-catalyzed carbon cathodes for Li–air batteries, Phys. Chem. Chem. Phys. 15 (2013) 11025–11037, https://doi.org/10.1039/c3cp51056e.
[39] M. Gastaldi, F. Gambino, H. Darjazi, A. Jouhara, S. Malburet, M. Zanetti, G. Saracco, G.A. Elia, C. Gerbaldi, Dry extrusion of poly(ethylene oxide)-polycarbonate all-solid-state electrolytes for Li-metal batteries: effect of UV-crosslinking on the electrochemical performance, Mater. Today Energy 52 (2025) 101947, https://doi.org/10.1016/j.mtener.2025.101947.
[40] Y.-C. Jung, M.-S. Park, D.-H. Kim, M. Ue, A. Eftekhari, D.-W. Kim, Room-temperature performance of Poly(Ethylene ether Carbonate)-Based solid polymer electrolytes for all-solid-state lithium batteries, Sci. Rep. 7 (2017) 17482, https://doi.org/10.1038/s41598-017-17697-0.
[41] B. Sun, J. Mindemark, K. Edström, D. Brandell, Polycarbonate-based solid polymer electrolytes for Li-ion batteries, Solid State Ionics 262 (2014) 738–742, https://doi.org/10.1016/j.ssi.2013.08.014.
[42] D. Bao, W. Zhao, Z. Li, Y. Tao, Y. Zhong, Z. Tang, Z. Gao, H. Wang, H. Zhang, X. Sun, A solid-like succinonitrile-based polymer electrolyte with superior mechanical strength for high performance lithium metal batteries, J. Energy Storage 91 (2024) 112016, https://doi.org/10.1016/j.est.2024.112016.
[43] D. Lin, P.Y. Yuen, Y. Liu, W. Liu, N. Liu, R.H. Dauskardt, Y. Cui, A silica-aerogel-reinforced composite polymer electrolyte with high ionic conductivity and high modulus, Adv. Mater. 30 (2018) 1802661, https://doi.org/10.1002/adma.201802661.
[44] Z. Li, J. Mindemark, D. Brandell, Y. Tominaga, A concentrated poly(ethylene carbonate)/poly(trimethylene carbonate) blend electrolyte for all-solid-state Li battery, Polym. J. 51 (2019) 753–760, https://doi.org/10.1038/s41428-019-0184-5.
[45] Q. Zhang, K. Liu, F. Ding, W. Li, X. Liu, J. Zhang, Safety-reinforced succinonitrile-based electrolyte with interfacial stability for high-performance lithium batteries, ACS Appl. Mater. Interfaces 9 (2017) 29820–29828, https://doi.org/10.1021/acsami.7b09119.
[46] B. Sun, C. Xu, J. Mindemark, T. Gustafsson, K. Edström, D. Brandell, At the polymer electrolyte interfaces: the role of the polymer host in interphase layer formation in Li-batteries, J. Mater. Chem. A 3 (2015) 13994–14000, https://doi.org/10.1039/C5TA02485D.
[47] X. Zhang, C. Fu, S. Cheng, C. Zhang, L. Zhang, M. Jiang, J. Wang, Y. Ma, P. Zuo, C. Du, Y. Gao, G. Yin, H. Huo, Novel PEO-based composite electrolyte for low-temperature all-solid-state lithium metal batteries enabled by interfacial cation-assistance, Energy Storage Mater. 56 (2023) 121–131, https://doi.org/10.1016/j.ensm.2022.12.048.